DIFFERENTIABLE METRIC FOR DISCOVERING FINITE GROUPS AND THEIR UNITARY REPRESENTATIONS

Anonymous authors
Paper under double-blind review

ABSTRACT

Discovering group structures within data is a significant challenge with broad implications across various scientific domains. The main hurdle stems from the non-differentiable nature of group axioms, hindering their seamless integration into deep learning frameworks. To address this, we introduce a novel differentiable approach that leverages the representation theory of finite groups. Our method employs a unique neural network architecture that models interactions between group elements as multiplications of their matrix representations, coupled with a regularizer that promotes unitarity of these matrices. Furthermore, our model implicitly defines a complexity metric that prioritizes the discovery of group structures. In numerical evaluation, our method successfully recovers group operations from a limited number of observations as well as accurately learning their unitary representations. This work establishes a new avenue for uncovering groups within data, with potential applications in diverse fields, including automatic symmetry discovery in deep learning.

1 INTRODUCTION

The discovery of algebraic structures, and particularly groups, has been foundational to advancements across numerous scientific disciplines. In mathematics, groups offer a powerful language for expressing symmetries and transformations, underpinning fields such as abstract algebra, geometry, topology, and number theory. In physics, group theory is indispensable for understanding the fundamental laws of nature, from classifying elementary particles to formulating quantum field theory. In computer science, groups play a key role in cryptography, coding theory, and algorithm design. Even within deep learning, group theory finds practical applications in designing symmetry-respecting architectures (e.g., convolutional and equivariant neural networks), resulting in models with fewer parameters and enhanced generalization, as well as extending deep learning to non-Euclidean spaces (Bronstein et al., 2021).

Despite their pervasive significance, uncovering group structures within data remains a challenge, often demanding expert human insight and intuition. A central hurdle is that the defining criterion for groups — the group axioms — is inherently non-differentiable, hindering its direct integration into deep learning frameworks.

In this work, we present a differentiable method for discovering groups and their representations by leveraging the representation theory of finite groups. We employ a novel architecture that models interactions between set elements as multiplications of their matrix representations, and a regularizer that promotes unitarity of these matrices. This approach inherently encodes the axioms of group operations, which instills a strong inductive bias towards discovering groups. This work demonstrates that the criterion for groups can be effectively embedded within a differentiable framework, opening new avenues for discovering algebraic structures within data.

2 GROUPS AND REPRESENTATIONS

Algebraic structures, *i.e.* sets equipped with operations adhering to specific axioms, offer a powerful framework for studying abstract mathematical objects and their interactions. Among these structures, groups serve as foundational building blocks in abstract algebra, underpinning the construction of more complex algebraic entities such as rings and fields. Additionally, the well-developed theory

of group representations offers a powerful tool for analyzing and understanding group structures. In this section, we provide a concise overview of groups and their representations, focusing on key concepts relevant to our work.

Groups A group $(G, \circ)$ is a set G with a binary operation $\circ$ that satisfies four axioms: Closure: $\forall a, b \in G$, $a \circ b \in G$. Associativity: $(a \circ b) \circ c = a \circ (b \circ c)$. Identity: There exists an identity element $e \in G$ such that for all $g \in G$, $g \circ e = e \circ g = g$. Inverse: For every $g \in G$, there exists a unique inverse element g^{-1} such that $g \circ g^{-1} = g^{-1} \circ g = e$.

Representations A representation of a group $(G, \circ)$ on a vector space V is a *group homomorphism* $\varrho \colon G \to \mathrm{GL}(V)$ that preserves the group structure: *i.e.*

$$\varrho(g_1 \circ g_2) = \varrho(g_1)\varrho(g_2), \qquad \forall g_1, g_2 \in G. \tag{1}$$

In essence, it maps each group element to an invertible linear transformation on the vector space, ensuring that the composition of transformations mirrors the group operation. For a finite-dimensional vector space of dimension n, we can choose a basis to identify $GL(V)$ as $GL(n, K)$, the group of $n \times n$ invertible matrices over the field K.

Unitary Representations A representation ϱ of a group $(G, \circ)$ is called *unitary* if for every $g \in G$, $\varrho(g)$ is a unitary transformation, *i.e.* preserves the inner product. This property makes unitary representations particularly well-behaved and amenable to analysis. Notably, the *Unitarity Theorem* guarantees that for many important classes of groups, such as compact and finite groups, every finite-dimensional representation is equivalent to a unitary one. Unitary representations naturally arise in the study of quantum systems, and have deep connections to other areas of mathematics, e.g., harmonic analysis and operator algebras.

Irreducible Representations A representation is considered *reducible* if it can be decomposed into a direct sum of smaller representations via a similarity transform, leading to a block-diagonal matrix form where each block corresponds to a simpler representation. *Irreducible* representations (irreps), on the other hand, cannot be further decomposed and serve as the fundamental building blocks for constructing all possible group representations.

Regular Representations Every group $(G, \circ)$ possesses an inherent action on itself that can be viewed as a permutation, where each group element rearranges the other elements. The *regular* representation uses the permutation's basis vectors to construct a linear representation. It is decomposible into a direct sum of the *complete* set of irreps, where each irrep appears with a multiplicity equal to its dimension. Moreover, its trace, also known as *character*, is a simple function:

$$\mathrm{Tr}[\varrho(g)] = n \;\text{ if } g = e, \;\; 0 \;\text{ otherwise.} \tag{2}$$

Real vs Complex Representations Complex representations ($K = \mathbb{C}$) provide a rich mathematical framework for analyzing group structures in representation theory. We utilize this framework to establish the theoretical foundations of our approach in Sections 4 and 5. However, for finite groups, real representations ($K = \mathbb{R}$) often suffice in practice,[1]offering advantages in implementation and visualization. Our empirical results in Sections 6 and 7 thus utilize real representations.

3 Background

Binary Operation Completion (BOC) We employ BOC (Power et al., 2022) as the setting for our study. BOC involves completing a "multiplication" table (Cayley table) of a binary operation over a finite set of abstract symbols. This problem setting isolates the core challenge of discovering group structures solely from element interactions, without confounding influence of other factors. This provides a crucial theoretical framework for analyzing structure learning in the discrete symbolic domain, analogous to the role of matrix completion in the continuous domain.

[1]For finite groups, every complex representation can be realized over the real numbers with a doubling of the dimension.

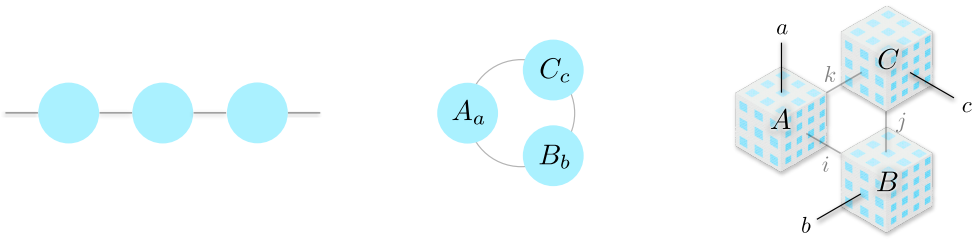

Figure 1: Illustration of matrix and tensor products. Nodes are factors and edges are indices. (Left) Matrix product. (Middle) Matrix product with trace operation. (Right) HyperCube product.

Matrix Completion Matrix completion involves filling in missing entries of a partially observed matrix with low-rank assumption on the underlying complete matrix. Classical approaches often leverage this assumption through explicit rank constraints (Burer and Monteiro, 2003) or by minimizing the nuclear norm as a convex surrogate for rank (Fazel et al., 2001; Candès and Recht, 2009; Recht et al., 2010; Candes and Tao, 2010). Matrix completion serves as a theoretical foundation for a wide array of applications, including recommender systems, data imputation, compressed sensing, and signal processing.

Implicit Complexity Metric Recent works demonstrated that deep matrix factorization networks with L_2 regularization (or small weight initialization) implicitly define a complexity metric that approximates rank: *e.g.*, nuclear or Schatten norm (Srebro et al., 2004; Gunasekar et al., 2017). Moreover, such implicit approaches have demonstrated superior performance in matrix completion compared to classical methods, particularly when dealing with limited data (Arora et al., 2019).

Our Contributions: Bridging the Gap While BOC shares many similarities with matrix completion, its discrete symbolic nature presents unique challenges. To bridge this gap, we linearize the problem into a tensor completion problem, and propose a novel solution grounded in the representation theory of finite groups: a tailored tensor-factorization architecture paired with a novel regularizer. This approach implicitly defines a complexity metric that serves as a differentiable surrogate for the group criterion, offering a learning-based approach for discovering group structures within data.

4 Modeling Framework

Notations and Definitions We use the following capital symbols for order-3 tensor factors: A, B, C. A_a denotes the matrix slice of A at the first index a and $A_a^\dagger$ denotes its conjugate transpose. $A_a B_b$ denotes the matrix product of A_a and B_b. Einstein convention is used throughout, where a repeated index implies contraction: *e.g.*, $A_a A_a^\dagger \equiv \sum_a A_a A_a^\dagger$, unless otherwise specified.

4.1 Linearized Framework: Binary Operations as Bilinear Maps

Consider a binary operation $\circ : S \times S \to S$ over a finite set S containing n elements with closure: *i.e.* $a \circ b = c$, where $a, b, c \in S$. To facilitate modeling, we linearize the problem by considering a homomorphism $\phi : (S, \circ) \to (V, \mathcal{D})$, where V is a vector space and $\mathcal{D} : V \times V \to V$ is a bilinear map over V, such that $\mathcal{D}(\phi(a), \phi(b)) = \phi(a \circ b)$. Concretely, by choosing the vector space $V = \mathbb{C}^n$ with a basis (for instance, encoding each element as a one-hot vector), the bilinear map $\mathcal{D}$ can be represented by an order-3 tensor $D \in \mathbb{C}^{n \times n \times n}$, whose entries are

$$D_{abc} = 1 \text{ if } a \circ b = c, \;\; 0 \text{ otherwise.} \tag{3}$$

where the elements of S are used as tensor indices for clarity. Hereafter, we will use D to denote the ground-truth data tensor to be learned by the model.

The linearized framework reveals that any binary operation over a finite set can be fully modeled by a bilinear map, or equivalently, by its tensor representation. Crucially, this framework transforms BOC into a tensor completion problem, where we recover the missing entries of D from the observed entries in the training set.

4.2 HyperCube Parameterization

To solve the tensor completion problem, we train a model tensor T to recover the data tensor D. However, the entries of T shouldn't be treated as independent model parameters. This would prevent the entries from utilizing the information of the other entries, leading to poor generalization.

To address this, we introduce HyperCube factorization (Fig. 1), which parameterizes the model tensor T as a product of three order-3 factors (*i.e. cubes*) $A, B, C \in \mathbb{C}^{n\times n\times n}$:

$$T_{abc} = \frac{1}{n}\,\mathrm{Tr}[A_a B_b C_c] = \frac{1}{n}\sum_{ijk} A_{aki} B_{bij} C_{cjk}. \tag{4}$$

This architecture employs matrix embeddings to represent the elements of the set S. Factors A and B serve as embedding dictionaries, mapping each element a and b to their respective matrix embeddings: A_a and B_b.[2] The interaction between a and b is then modeled as the matrix multiplication: $A_a B_b$. Finally, factor C acts as an *unembedding* dictionary, mapping this result back to S.

This architecture is inspired by the representation theory of finite groups, which similarly employs matrix multiplication to model group operations: eq (1). This has the key advantage of directly encoding the associativity axiom of groups through the associative property of matrix multiplication. This inherent encoding provides a crucial advantage for effectively capturing group structures.

Appendix F compares HyperCube to other common tensor factorization methods and demonstrates their limitations in capturing group structure, further highlighting the strengths of our approach.

4.3 HyperCube Regularizer

The model is trained by minimizing the following regularized objective:

$$\mathcal{L} = \mathcal{L}_o(T; D) + \epsilon\mathcal{H}(A, B, C), \tag{5}$$

where $\mathcal{L}_o$ is a differentiable loss on the model tensor T (*e.g.*, squared error over the training data) and $\mathcal{H}$ is the HyperCube regularizer, which penalizes the Jacobian of T with respect to the parameters:

$$\mathcal{H} \equiv \left\|\frac{\partial T}{\partial A}\right\|_F^2 + \left\|\frac{\partial T}{\partial B}\right\|_F^2 + \left\|\frac{\partial T}{\partial C}\right\|_F^2 = \frac{1}{n}\,\mathrm{Tr}\left[A_a^\dagger A_a B_b B_b^\dagger + B_b^\dagger B_b C_c C_c^\dagger + C_c^\dagger C_c A_a A_a^\dagger\right], \tag{6}$$

which can be viewed as a *dual* to the standard L_2 regularization: $\|A\|_F^2 + \|B\|_F^2 + \|C\|_F^2$. In subsequent sections, we demonstrate that eq (6) encourages the factors to learn full-rank, unitary matrix embeddings. This stands in contrast to L_2 regularization, which promotes low-rank solutions.

This bias toward unitary embeddings leverages the *Unitarity Theorem* of representation theory, which guarantees that for compact and finite groups, every finite-dimensional representation is equivalent to a unitary representation. Therefore, by biasing the model to consider only unitary matrix embeddings, we *significantly reduce the search space of possible solutions without loss of generality*. This bias aids in faster convergence and enhances the model's ability to generalize, as it focuses the learning process on a smaller, more relevant space of representations.

4.4 Internal Symmetry of Model

The over-parameterized eq (4) implies the presence of internal symmetries that leave the model unchanged. For instance, one can introduce arbitrary invertible matrices M_I, M_J, M_K and their inverses between the factors as $\tilde{A}_a = M_K^{-1} A_a M_I$, $\tilde{B}_b = M_I^{-1} B_b M_J$, and $\tilde{C}_c = M_J^{-1} C_c M_K$. These yield an equivalent parameterization of T, since $\mathrm{Tr}[\tilde{A}_a \tilde{B}_b \tilde{C}_c] = \mathrm{Tr}[A_a B_b C_c]$. These symmetry transformations can be understood as changing the internal basis coordinate to represent the factors.

Note that while the model loss $\mathcal{L}_o(T)$ is invariant under such coordinate changes, the regularizer $\mathcal{H}(A, B, C)$ is not. However, the regularizer is invariant under *unitary* basis changes, in which the introduced matrices are unitary, such that $MM^\dagger = M^\dagger M = I$. Therefore, the regularizer imposes a stricter form of symmetry. This leads to the following Proposition.

Proposition 4.1. *If A, B, C form the optimal solution of the regularized loss eq* (5)*, then any unitary basis changes leave the solution optimal, but non-unitary basis changes generally increase the loss.*

[2] This embedding process is closely related to the generalized Fourier transform on groups (See Appendix J).

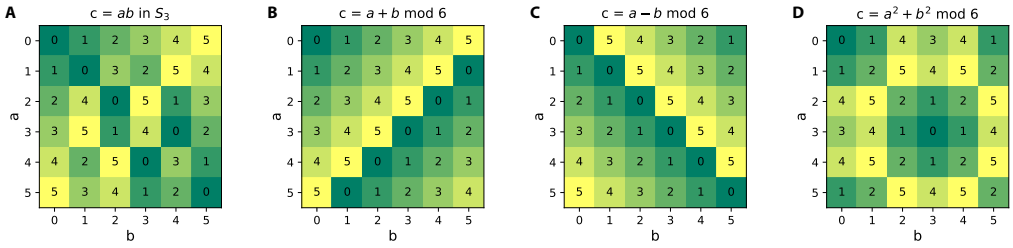

Figure 2: Multiplication tables (*i.e.* Cayley tables) of small binary operations: symmetric group S_3, modular addition, subtraction, and squared addition. Elements of S_3 are illustrated in Figure 8.

5 Analyzing HyperCube's Inductive Bias

While HyperCube eq (4) does not explicitly restrict the model's hypothesis space, the regularizer eq (6) induces a strong implicit bias on the model. In this section, we introduce key concepts for analyzing this inductive bias. See Appendix H for proofs.

Lemma 5.1 (Balanced Condition)**.** *At stationary points of eq* (5)*, imbalance terms vanish to zero:*

$$\xi_I = \xi_J = \xi_K = 0, \tag{7}$$

where $\xi_I = A_a^\dagger (C_c^\dagger C_c) A_a - B_b (C_c C_c^\dagger) B_b^\dagger$, $\xi_J = B_b^\dagger (A_a^\dagger A_a) B_b - C_c (A_a A_a^\dagger) C_c^\dagger$, *and* $\xi_K = C_c^\dagger (B_b^\dagger B_b) C_c - A_a (B_b B_b^\dagger) A_a^\dagger$ *are the imbalances across edge* i, j*, and* k*, respectively.*

The following statements demonstrate that the regularizer promotes a unitarity condition.

Definition 5.2 (Contracted Unitarity)**.** A factor A is *C-unitary* if it satisfies the following: $A_a A_a^\dagger$, $A_a^\dagger A_a \propto I$ (*with* contracting the repeated index a).

Proposition 5.3. *C-unitary factors satisfy the balanced condition eq* (7)*, given that they share a common scalar multiple of the identity matrix: i.e.*

$$A_a A_a^\dagger = A_a^\dagger A_a = B_b B_b^\dagger = B_b^\dagger B_b = C_c C_c^\dagger = C_c^\dagger C_c \equiv n\alpha^2 I, \tag{8}$$

Lemma 5.4. *Under the fixed Frobenius norm, all C-unitary factors are stationary points of the regularizer* $\mathcal{H}$*.*

Lemma 5.4 indicates that $\mathcal{H}$ effectively promotes C-unitarity as well as minimizing the Frobenius norm. Remarkably, we also observe a stronger form of unitarity in the converged solutions.

Definition 5.5 (Slice Unitarity)**.** A factor A is *S-unitary* if every matrix slice of A is a scalar multiple of an unitary matrix: *i.e.* $A_a A_a^\dagger = A_a^\dagger A_a \equiv \alpha_{A_a}^2 I$ (*without* contracting the repeated index a).

Observation 5.6. *When optimizing the regularized loss eq* (5)*, C-unitary solutions are consistently achieved via S-unitarity, in which eq* (8) *reduces to* $\sum_a \alpha_{A_a}^2 = \sum_b \alpha_{B_b}^2 = \sum_c \alpha_{C_c}^2 = n\alpha^2$.

Although the exact mechanism driving S-unitarity remains an open question, this observation highlights the strong inductive bias towards unitarity imposed by the HyperCube regularizer.

6 Analysis on Small-Scale Experiments

We begin by evaluating HyperCube on the small-scale binary operations shown in Figure 2. We provide detailed analysis of the learning process (Section 6.1) and the learned embedding (Section 6.2). This analysis reveals the central role of unitarity bias in uncovering group structures and the exact matrix representations of the underlying groups.

6.1 Learning Dynamics on Symmetric Group S_3

Figure 3 compares the effect of different regularization strategies on the model's learning dynamics on the symmetric group S_3 with 60% of the Cayley table sampled as training data. (See also Figure 14 for a direct visualization of the evolution of the model tensor and parameters.) Similar analysis on the learning of the modular addition operation is presented in Figure 17 and 18.

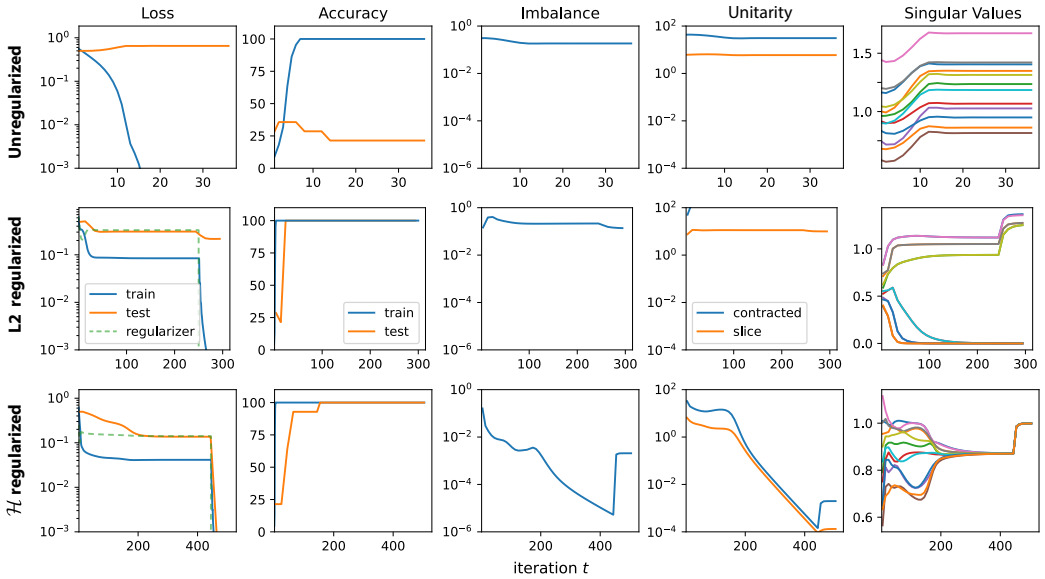

Figure 3: Optimization trajectories on the S_3 dataset with 60% training data fraction. (Top) Unregularized, (Middle) L_2-regularized, and (Bottom) $\mathcal{H}$-regularized training. Column 3 shows the average imbalance $(\|\xi_I\|_F^2 + \|\xi_J\|_F^2 + \|\xi_K\|_F^2)^{1/2}$, and column 4 shows deviation from C-unitarity $\|\sum_a A_a A_a^\dagger/n - \alpha^2 I\|_F^2$ and S-unitarity $\|A_a A_a^\dagger - \alpha_{A_a}^2 I\|_F^2$, averaged over all factors and slices. Column 5 shows normalized singular values of unfolded factors A, B, C.

In the absence of regularization, the model quickly memorizes the training dataset, achieving perfect training accuracy, but fails to generalize to the test dataset. Also, the singular values of the unfolded factors remain largely unchanged during training, indicating minimal internal structural changes.

Under $\mathcal{H}$ regularization, the model also rapidly memorizes the training data, but then continues to improve on the test set. A critical turning point is observed around $t \approx 200$, marked by a sudden collapse of the singular values towards a common value, signifying convergence to a unitary solution. Simultaneously, the C/S-unitarity and imbalance measures rapidly decrease to zero. This internal restructuring coincides with a substantial improvement in test performance, achieving 100% test accuracy, highlighting its crucial role in enabling generalization. Notably, when the regularization coefficient ϵ drops to 0 around $t = 450$, both the train and test losses plummet to 0, confirming perfect recovery of D.

In contrast, under L_2 regularization, the model converges to a low-rank solution, as evidenced by a portion of the singular values decaying to zero. Although it manages to achieve perfect test accuracy in this specific case,[3] L_2 regularization fails to reduce the test loss to zero, indicating imperfect recovery of D. Figure 4 further confirms these findings, demonstrating that only $\mathcal{H}$-regularization accurately recovers the group operation, while the L_2-regularized solution deviates significantly from D. This result underscores the importance of learning full-rank solutions in recovering group operations.

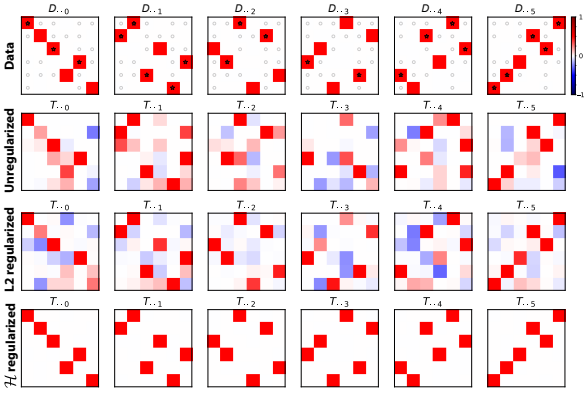

Figure 4: Model tensor T trained on the S_3 dataset. Training data are marked by stars (1s) and circles (0s).

6.2 HyperCube Learns Unitary Group Representations

[3]This is not always the case. For example, L_2 regularization only achieves ∼60% test accuracy in the modular addition task. See Figure 17.

We analyze the structure of the learned factors by utilizing unitary basis change (Section 4.4). The results are visualized in Figure 15. While the raw factor values may appear unstructured (top panel), a simple basis change reveals remarkable properties (middle panel).

First, the learned factors share the same embedding: $A_g = B_g = C_g^\dagger, \forall g \in G$. Furthermore, multiplication of the factor slices respects the underlying group operation (Figure 16): $A_{g_1} A_{g_2} = A_{g_1 \circ g_2}$, demonstrating the group homomorphism property from eq (1). The slices are also verifiably unitary matrices. These properties collectively imply that the learned factors form a unitary matrix representation ϱ of the group:

$$A_g = B_g = C_g^\dagger = \varrho(g). \tag{9}$$

Further structures are revealed in a block-diagonalizing basis (bottom panel), where the factors reveal the *complete set of irreps* contained in the regular representation of the group, including the trivial (1-dim), sign (1-dim), and duplicate standard representations (2-dim). The trace of the factor slices also satisfies eq (2), confirming that ϱ is indeed a regular representation of the group.

Key Operating Mechanism These results reveal the operating mechanism of HyperCube on groups. Applying eq (9) and the homomorphism property of ϱ, the model eq (4) can be expressed as

$$T_{abc} = \frac{1}{n} \operatorname{Tr}[\varrho(a)\varrho(b)\varrho(c)^\dagger] = \frac{1}{n} \operatorname{Tr}[\varrho(a \circ b \circ c^{-1})]. \tag{10}$$

Due to the unitarity of ϱ, slices of factor C correspond to the inverse representation: $C_g = \varrho(g)^\dagger = \varrho(g^{-1})$. Notably, since ϱ is a regular representation of the group eq (2), this result exactly reproduces the data tensor, $T_{abc} = D_{abc}$, because $a \circ b \circ c^{-1} = e$ is equivalent to $a \circ b = c$ in eq (3). This mechanism universally applies for all finite groups. This insight leads to the following conjecture:

Conjecture 6.1. *Let D represent a group operation table. Then, given the constraint $T = D$, the unitary group representation eq* (9) *describes the unique minimizer of HyperCube Regularizer eq* (6) *up to unitary basis changes, whose minimum value is $\mathcal{H}^*(D) = 3\|D\|_F^2 = 3n^2$.*

Shared-Embedding Eq (9) reveals that, for group operations, the same embedding is used across all symbol positions. This motivates tying the embeddings across factors, resulting in a parameter-efficient model tailored for learning group operations: HyperCube-SE (shared embedding).

6.3 Discovering Unitary Representations Beyond True Groups

We analyze HyperCube trained on the remaining small operation tasks from Figure 2. The model accurately recovers the underlying operations from a small subset of examples in each case. Interestingly, the model learns closely related representations across these tasks (Figure 19), even when the operations deviate from strict group axioms.

Modular Addition ($a + b = c$) forms the cyclic group C_6. As expected, HyperCube learns the regular representation $\varrho(g)$ of C_6 in its factors, as described by eq (9).

Modular Subtraction ($a - b = c$) violates associativity and therfore is not a true group. Surprisingly, HyperCube still learns the same representation as addition but with transposed factors: $A_g^\dagger = B_g = C_g = \varrho(g)$. This reflects the equivalence: $a - b = c \Leftrightarrow a = b + c$.

Modular Squared Addition ($a^2 + b^2 = c$) violates the inverse axiom. Still, HyperCube learns the same representation as addition for elements with unique inverses (e.g., $0, 3$). For others, it learns *duplicate* representations reflecting the periodicity of squaring modulo: *e.g.*, $A_2 = A_4$ since $2^2 = 4^2 (\text{mod } 6)$.

These results highlight the remarkable flexibility of HyperCube's inductive bias: Even for *group-like* operations (i.e., those deviating from strict group axioms), HyperCube often discovers meaningful unitary representations and recovers the full Cayley table. This finding highlights the potential of unitary representations as a powerful tool for understanding binary operations beyond the confines of traditional group theory.

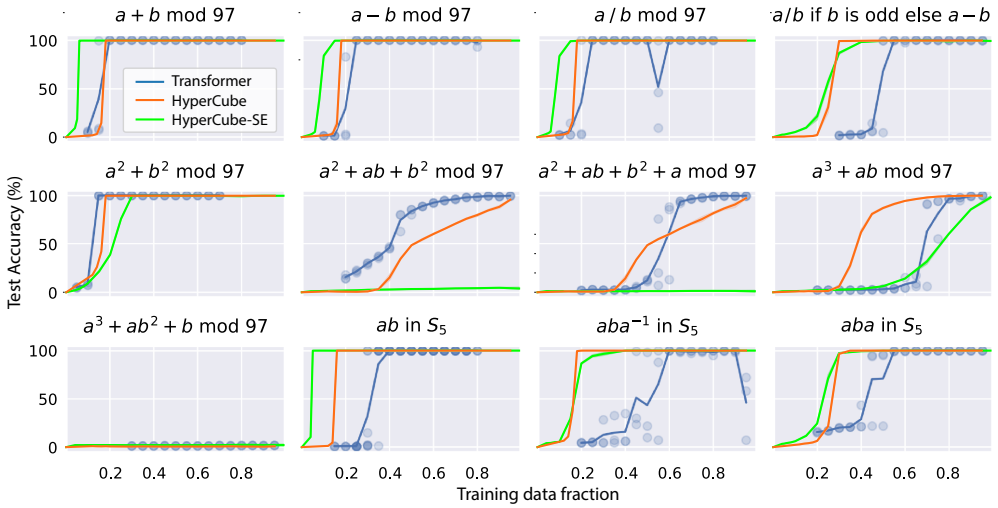

Figure 5: Generalization performance (test accuracy) of HyperCube and HyperCube-SE shown as functions of training data fraction across a diverse set of BOC tasks. The results of the Transformer baseline from Power et al. (2022) are also shown for comparison.

7 Results on Diverse BOC Tasks

We evaluate HyperCube and HyperCube-SE on diverse BOC datasets from Power et al. (2022), encompassing a wide spectrum of group and non-group operations (details in Appendix B). These problems are significantly larger than our previous examples, with dimensions ranging from $n = 97$ to 120. Figure 5 plots the test accuracy of models as functions of training data fraction over various BOC tasks.

7.1 HyperCube Prioritizes Groups over Non-Group Operations

HyperCube exhibits a clear prioritization for learning operations that admit unitary representations. For these "simple" tasks, including group ($a + b$ and S_5) and *group-like* operations ($a - b$, a/b and $a^2 + b^2$), HyperCube demonstrates remarkable generalization, achieving perfect test accuracy with $\sim$18% of the data. This strong performance also extends to group conjugation operation (aba^{-1} in S_5), even though it lacks unitary representations. In contrast, for more "complex" operations, such as aba in S_5, conditional operations and high-order polynomials, HyperCube requires more data for effective generalization.

HyperCube-SE shows similar behavior with an even more focused prioritization on group structures. It distinguishes between group and *group-like* operations, requiring even less data for group operations to achieve perfect test accuracy ($\sim$5%). On *group-like* operations, it remains competitive with HyperCube in terms of test accuracy performance, despite being unable to recover the unitary representations due to the shared-embedding eq (9). Furthermore, HyperCube-SE exhibits even further diminished generalization than HyperCube on "complex" operations like high-order polynomials, which aligns with its focused prioritization of groups.

7.2 HyperCube's Implicit Complexity Metric

In the above analysis, we qualitatively categorized tasks as "simple" or "complex" without a concrete definition. To address this, we leverage the intrinsic metric implicitly defined by HyperCube. We formally define the complexity of an operation as the minimum regularizer loss, denoted $\mathcal{H}^*$, achieved when fitting its full Cayley table D (*i.e.*, under the constraint $T = D$).

This metric closely aligns with the intuitive notion of complexity (Figure 6). Group operations achieve the minimum complexity of $\mathcal{H}^* = 3\|D\|_F^2$, indicating their inherent simplicity within HyperCube. *Group-like* operations also achieve this minimum in HyperCube but incur increased com-

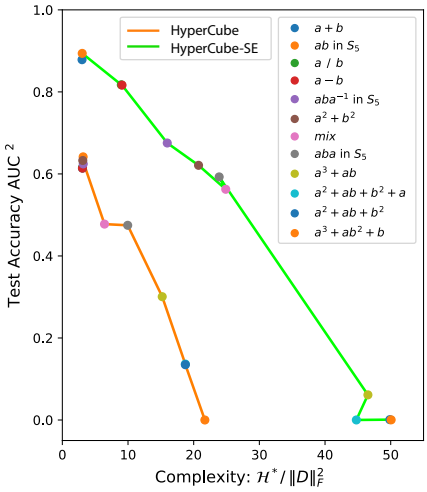

Figure 6: Complexity vs Generalizability (AUC $\equiv$ Area Under Curve).

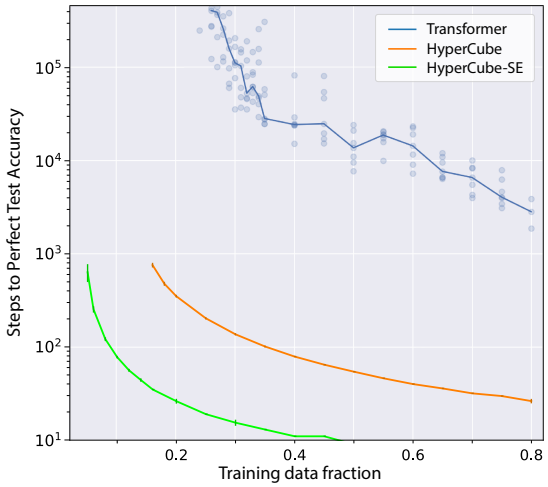

Figure 7: Number of training steps to achieve perfect test accuracy on the S_5 task.

plexity in HyperCube-SE, highlighting its focused inductive bias towards pure group structures. In contrast, more "complex" tasks, such as high-order polynomials, incur substantially higher complexity costs.

Figure 6 illustrates the generalization trend as a function of complexity, revealing a clear monotonic relationship: as task complexity increases, generalizability (measured by the total area under the test accuracy curve in Figure 5) decreases. This observation parallels the well-known relationship in matrix completion, where higher matrix rank (analogous to higher complexity) generally leads to poorer generalization and requires more data for effective learning. This underscores the critical role of our proposed complexity metric in determining the generalization bound for BOC.

7.3 Comparison to Transformer

Test accuracy performance Figure 5 also shows the Transformer baseline results from Power et al. (2022). Transformer exhibits a similar trend to HyperCube, requiring more data for more "complex" tasks. However, it tends to favor commutative operations (*e.g.*, $a+b$, a^2+ab+b^2) over non-commutative ones (*e.g.*, $a-b$, a^2+ab+b^2+a, and all S_5 tasks). This is likely due to Transformers sharing the vector embedding of symbols across all input locations (Power et al., 2022; Liu et al., 2022). Thus, unlike HyperCube, Transformer's inductive bias is not fully aligned with learning group structures. Overall, in terms of test accuracy, HyperCube exhibits comparable or slightly superior generalization to Transformer baselines across most tasks.

Learning speed HyperCube exhibits a dramatic advantage over Transformer in terms of learning speed (Figure 7). As reported by Power et al. (2022), Transformer's learning progress on BOC is remarkably slow, requiring orders of magnitude more time to generalize to the test set than to fit the training set. This phenomenon, known as "grokking," becomes exacerbated with less training data. This observation has been reproduced in several subsequent works exploring various deep learning architectures (Nanda et al., 2022; Liu et al., 2022; Chughtai et al., 2023).

In contrast, HyperCube exhibits exceptional learning speed, converging to perfect test accuracy 100 times faster than the Transformer baseline in most cases, while also requiring less data. HyperCube-SE, which employs shared-embedding of symbols similarly to Transformers, achieves an additional $10\times$ speedup and requires only 5% of the data for perfect generalization. This dramatic $1000\times$ improvement in learning speed demonstrates the effectiveness of HyperCube's inductive bias toward group structures.

8 Conclusion

In this work, we introduced a novel differentiable framework for discovering the structure of finite groups and their unitary representations. We demonstrated, via analysis and experiments, that our proposed model exhibits a strong priority towards learning group structures and their unitary representations. Furthermore, we identified an implicit complexity metric that emerges from our model, which quantifies the model's priority for discovering group structures and offers insights into the generalization capabilities of BOC learning. Crucially, this inductive bias is a universal one, directed towards the general algebraic structure of all groups, rather than being tailored to any specific group or symmetry.

This research opens new avenues for utilizing deep learning to automatically uncover group structures within data, a problem with significant implications across various scientific domains. Potential applications include: **Automatic Symmetry Discovery**: Identifying symmetries in complex systems, such as physical systems or molecular structures. **Representation Learning**: Learning meaningful representations of data that capture underlying algebraic relationships. **Algorithmic Reasoning**: Developing deep learning models capable of symbolic reasoning and algorithmic problem-solving.

Related Works Related to our work are prior works on group discovery, mostly in the context of discovering symmetries. However, most of them require an external source of information that provides the given symmetry structure. For example, Anselmi et al. (2019) utilize data augmentation with known orbit information; Forestano et al. (2023) similarly assumes an oracle that provides the orbit information; Yang et al. (2023) uses semi-supervised approach to infer orbit information; and Zhou et al. (2021) employ a meta-learning framework with the assumption of a shared group convolution structure across tasks. In contrast, our approach derives a universal bias towards the general algebraic structure of groups, rather than being tailored to specific symmetries. Therefore, it is complementary to and can be used in conjunction with these other methods.

Scalability HyperCube's use of tensor factors can incur substantial memory and computational costs, scaling as $O(n^3)$. However, efficient parallelization of `einsum` operations allows for near-constant run-time complexity on GPUs (Appendix E). Furthermore, we demonstrate that the memory and compute cost can be effectively reduced to $O(n^2)$ by constraining the embeddings to band-diagonal matrices (Appendix G), highlighting the potential for scaling HyperCube to larger problems.

Limitations Our analysis primarily focused on BOC tasks and requires knowing the size of the group, n. While not directly applicable to continuous Lie groups, we believe an analogous method can be developed to encode the axioms of Lie algebras in a differentiable way.

Open Questions This work raises several open questions for future studies, such as deriving exact generalization bounds for BOC and formally proving the optimality of unitary representations (Observation 5.6 and Conjecture 6.1). Extending our approach to handle multiple symbols and types of operations beyond binary operations would further broaden its applicability.

Acknowledgments

References

Anselmi, F., Evangelopoulos, G., Rosasco, L., and Poggio, T. (2019). Symmetry-adapted representation learning. *Pattern Recognition*, 86:201–208.

Arora, S., Cohen, N., Hu, W., and Luo, Y. (2019). Implicit Regularization in Deep Matrix Factorization. arXiv:1905.13655 [cs, stat].

Burer, S. and Monteiro, R. D. (2003). A nonlinear programming algorithm for solving semidefinite programs via low-rank factorization. *Mathematical Programming*, 95(2):329–357.

Candes, E. J. and Tao, T. (2010). The Power of Convex Relaxation: Near-Optimal Matrix Completion. *IEEE Transactions on Information Theory*, 56(5):2053–2080.

Candès, E. J. and Recht, B. (2009). Exact Matrix Completion via Convex Optimization. *Foundations of Computational Mathematics*, 9(6):717–772.

Chughtai, B., Chan, L., and Nanda, N. (2023). Neural Networks Learn Representation Theory: Reverse Engineering how Networks Perform Group Operations. In *ICLR 2023 Workshop on Physics for Machine Learning*.

Fazel, M., Hindi, H., and Boyd, S. (2001). A rank minimization heuristic with application to minimum order system approximation. In *Proceedings of the 2001 American Control Conference. (Cat. No.01CH37148)*, volume 6, pages 4734–4739 vol.6. ISSN: 0743-1619.

Forestano, R. T., Matchev, K. T., Matcheva, K., Roman, A., Unlu, E., and Verner, S. (2023). Deep Learning Symmetries and Their Lie Groups, Algebras, and Subalgebras from First Principles. arXiv:2301.05638 [hep-ph, physics:physics].

Gunasekar, S., Woodworth, B. E., Bhojanapalli, S., Neyshabur, B., and Srebro, N. (2017). Implicit Regularization in Matrix Factorization. In *Advances in Neural Information Processing Systems*, volume 30. Curran Associates, Inc.

Kawaguchi, K. (2016). Deep learning without poor local minima. In *Advances in neural information processing systems*, pages 586–594.

Liu, Z., Kitouni, O., Nolte, N., Michaud, E. J., Tegmark, M., and Williams, M. (2022). Towards Understanding Grokking: An Effective Theory of Representation Learning. In *Advances in Neural Information Processing Systems*.

Nanda, N., Chan, L., Lieberum, T., Smith, J., and Steinhardt, J. (2022). Progress measures for grokking via mechanistic interpretability. In *The Eleventh International Conference on Learning Representations*.

Power, A., Burda, Y., Edwards, H., Babuschkin, I., and Misra, V. (2022). Grokking: Generalization Beyond Overfitting on Small Algorithmic Datasets.

Recht, B., Fazel, M., and Parrilo, P. A. (2010). Guaranteed Minimum-Rank Solutions of Linear Matrix Equations via Nuclear Norm Minimization. *SIAM Review*, 52(3):471–501.

Saxe, A. M., McClelland, J. L., and Ganguli, S. (2014). Exact solutions to the nonlinear dynamics of learning in deep linear neural networks. arXiv:1312.6120 [cond-mat, q-bio, stat].

Srebro, N., Rennie, J., and Jaakkola, T. (2004). Maximum-Margin Matrix Factorization. In *Advances in Neural Information Processing Systems*, volume 17. MIT Press.

Tucker, L. R. (1966). Some mathematical notes on three-mode factor analysis. *Psychometrika*, 31(3):279–311.

Yang, J., Walters, R., Dehmamy, N., and Yu, R. (2023). Generative Adversarial Symmetry Discovery. arXiv:2302.00236 [cs].

Zhou, A., Knowles, T., and Finn, C. (2021). Meta-Learning Symmetries by Reparameterization. arXiv:2007.02933 [cs, stat].

A Training Procedure

The factor tensors are initialized with entries randomly drawn from a normal distribution: $\mathcal{N}(0, 1/\sqrt{n})$. We employ full-batch gradient descent to optimize the regularized loss with learning rate of 0.5 and momentum of 0.5. For the small scale experiments in Section 6, the HyperCube regularizer coefficient is set to $\epsilon = 0.1$. For the larger scale experiments in Section 7, we use $\epsilon = 0.05$ for HyperCube and $\epsilon = 0.01$ for HyperCube-SE. See Appendix D for a discussion of hyperparameter sensitivity. Each experiment quickly runs within a few minutes on a single GPU.

ϵ-scheduler To overcome the limitations in standard regularized optimization, which often prevents full convergence to the ground truth (D), we employ ϵ-scheduler: Once the model demonstrates sufficient convergence (*e.g.*, the average imbalance falls below a threshold of 10^{-5}), the scheduler sets the regularization coefficient ϵ to 0. This allows the model to fully fit the training data. The effect of ϵ-scheduler on convergence is discussed in Appendix H.3.

The main implementation of HyperCube is shown below. Code repository is available at `https://anonymous.4open.science/r/DeepTensorFactorization4GroupRep-EB92/`

```python
import torch

def HyperCube_product(A,B,C):
    return torch.einsum('aij,bjk,cki->abc', A,B,C) / A.shape[0]

def HyperCube_regularizer(A,B,C):
    def helper(M,N):
      MM = torch.einsum('aim,aij->mj', M,M)
      NN = torch.einsum('bjk,bmk->jm', N,N)
      return torch.einsum('mj,jm->', MM, NN)
    return (helper(A,B) + helper(B,C) + helper(C,A) ) / A.shape[0]
```

B List of Binary Operations

Here is the list of binary operations from Power et al. (2022) that are used in Section 7 (with $p = 97$).

- (add) $a \circ b = a + b \pmod p$ for $0 \le a, b < p$. (Cyclic Group)
- (sub) $a \circ b = a - b \pmod p$ for $0 \le a, b < p$.
- (div) $a \circ b = a/b \pmod p$ for $0 \le a < p, 0 < b < p$.
- (cond) $a \circ b = [a/b \pmod p$ if b is odd, otherwise $a - b \pmod p]$ for $0 \le a, b < p$.
- (quad1) $a \circ b = a^2 + b^2 \pmod p$ for $0 \le a, b < p$.
- (quad2) $a \circ b = a^2 + ab + b^2 \pmod p$ for $0 \le a, b < p$.
- (quad3) $a \circ b = a^2 + ab + b^2 + a \pmod p$ for $0 \le a, b < p$.
- (cube1) $a \circ b = a^3 + ab \pmod p$ for $0 \le a, b < p$.
- (cube2) $a \circ b = a^3 + ab^2 + b \pmod p$ for $0 \le a, b < p$.
- (ab in S_5) $a \circ b = a \cdot b$ for $a, b \in S_5$. (Symmetric Group)
- (aba^{-1} in S_5) $a \circ b = a \cdot b \cdot a^{-1}$ for $a, b \in S_5$.
- (aba in S_5) $a \circ b = a \cdot b \cdot a$ for $a, b \in S_5$.

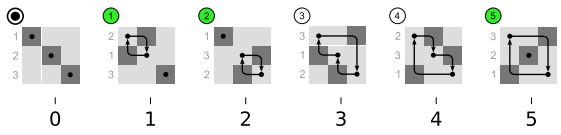

Figure 8: Elements of the symmetric group S_3 illustrated as permutations of 3 items. Green color indicates *odd* permutations, and white indicates *even* permutations. Adapted from `https://en.wikipedia.org/wiki/Symmetric_group`.

C UNDERSTANDING HYPERCUBE REGULARIZER

To gain an intuitive understanding of the HyperCube regularizer, consider a simplified, scalar HyperCube model $t = abc$ with $a, b, c \in \mathbb{R}$. Minimizing the L_2 regularizer $a^2 + b^2 + c^2$ subject to the data constraint $t = 1$ yields the usual balanced condition:

$$a = b = c = 1. \tag{11}$$

In contrast, the HyperCube regularizer eq (6) becomes:

$$\begin{aligned}\mathcal{H}(a, b, c) &= \left(\frac{\partial t}{\partial a}\right)^2 + \left(\frac{\partial t}{\partial b}\right)^2 + \left(\frac{\partial t}{\partial c}\right)^2 \\ &= \left(\frac{t}{a}\right)^2 + \left(\frac{t}{b}\right)^2 + \left(\frac{t}{c}\right)^2 \\ &= \tilde{a}^2 + \tilde{b}^2 + \tilde{c}^2,\end{aligned} \tag{12}$$

where, given the constraint $t = 1$, we defined the substitute variables as $\tilde{a} \equiv 1/a$, $\tilde{b} \equiv 1/b$, and $\tilde{c} \equiv 1/c$. Minimizing eq (12) subject to the constraint $\tilde{a}\tilde{b}\tilde{c} = 1$ yields the balanced condition $\tilde{a} = \tilde{b} = \tilde{c} = 1$, or equivalently,

$$\frac{1}{a} = \frac{1}{b} = \frac{1}{c} = 1. \tag{13}$$

This is the reciprocal of the L_2 regularizer's balanced condition eq (11), although the solutions are identical in this scalar case. This example demonstrates that the HyperCube regularizer instills a "reciprocal" bias compared to the L_2 regularizer.

C.0.1 BALANCED CONDITION FOR L_2 REGULARIZATION

In contrast to the balanced condition of HyperCube regularizer eq (7), L_2 Regularization yields a simpler balanced condition

$$\xi_I^{L_2} = \xi_J^{L_2} = \xi_K^{L_2} = 0, \tag{14}$$

where $\xi_I^{L_2} = A_a^\dagger A_a - B_b B_b^\dagger$, $\xi_J^{L_2} = B_b^\dagger B_b - C_c C_c^\dagger$, and $\xi_K^{L_2} = C_c^\dagger C_c - A_a A_a^\dagger$. Analogous matrix-version of this balanced condition has been derived in prior works for deep linear networks (Arora et al., 2019; Saxe et al., 2014), which leads to balanced singular modes across the layers: *i.e.* the adjacent layers share the same singular values and singular vector matrices. Crucially, this result shows how L_2 regularization promotes low-rank solutions, since the L_2 loss on individual factors is equivalent to penalizing $\sum_i |\sigma_i|^{2/L}$, where σ_i is the singular value of the end-to-end input-output map, and L is the number of layers. This is called the Schatten norm minimization.

D HYPERPARAMETER SENSITIVITY ANALYSIS

We tested HyperCube across a wide range of hyperparameter settings, including learning rate, regularization coefficient, and weight initialization scale. Figure 9 shows the final test accuracy and Figure 10 shows the number of training steps to achieve 100% test accuracy across a subset of tasks from Appendix B under a fixed training budget of 1000 training steps.

HyperCube exhibits robust performance over the range of hyperparameter settings. Notably, increasing the learning rate or regularization coefficient primarily raises the convergence speed without significantly affecting the final test accuracy. The learning dynamics starts to become unstable at large learning rate (lr $= 1.5$) or regularization coefficient ($\epsilon = 0.1$). The weight initialization scale has no effect on either the final test accuracy or the convergence speed.

This robustness, particularly to weight initialization scale and regularization strength, is noteworthy. Deep neural networks exhibit a saddle point with zero Hessian at zero weights (Kawaguchi, 2016) which becomes a local minimum under L_2 regularization. This local minimum can cause the network weights to collapse to zero when initialized with small values or under strong regularization. (This mechanism also promotes low-rank solutions in L_2-regularized deep neural networks.)

In contrast, HyperCube's quartic regularization loss, also featuring zero Hessian at zero weights, maintains the saddle point at zero. The absence of local minimum at zero prevents weight collapse, contributing to significantly robust learning dynamics and promoting the emergence of full-rank unitary representations in HyperCube.

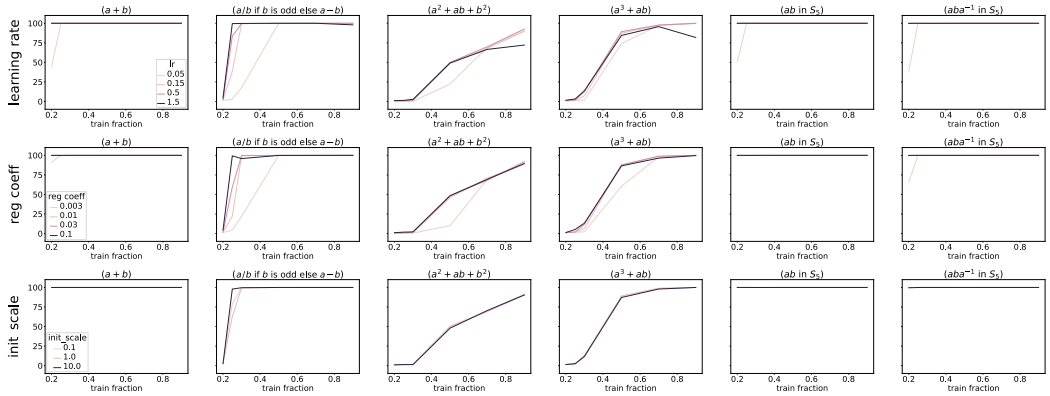

Figure 9: **Test accuracy vs Hyperparameters** : (Top) learning rate, (Middle) regularization strength, and (Bottom) weight initialization scale. Trained under a fixed training budget of 1000 steps. Default hyperparameter setting: lr $= 0.5$, reg coeff $\epsilon = 0.05$, init scale $= 1.0$.

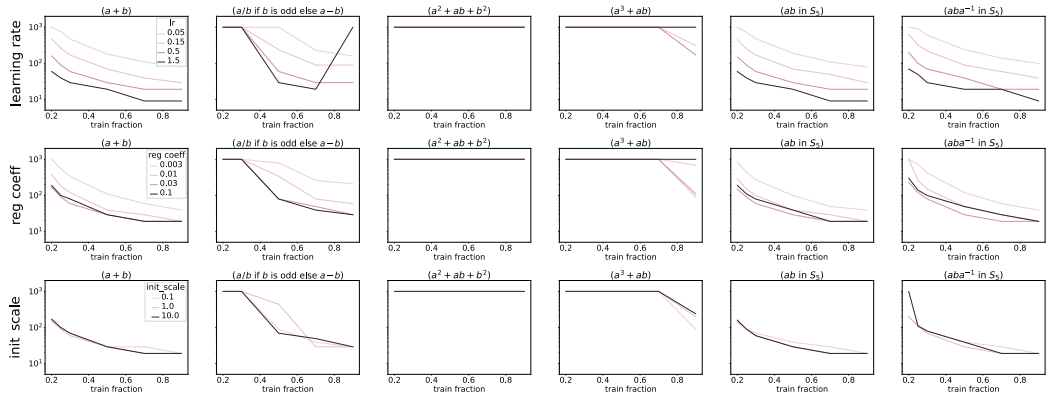

Figure 10: **Steps to 100% accuracy vs Hyperparameters** : Same settings as Fig 9, but showing the number of training steps to achieve 100% test accuracy.

E Run-time Complexity

We empirically evaluate the run-time complexity of HyperCube. As expected, CPU execution time scales as $O(n^3)$. However, due to the efficient parallelization of `einsum` operations in PyTorch (See Appendix A), GPU execution time remains nearly constant with increasing n (up to $n = 200$, the maximum size that fits in the 16GB memory of a Tesla V100 GPU). This demonstrates the practical efficiency of HyperCube when leveraging GPU acceleration.

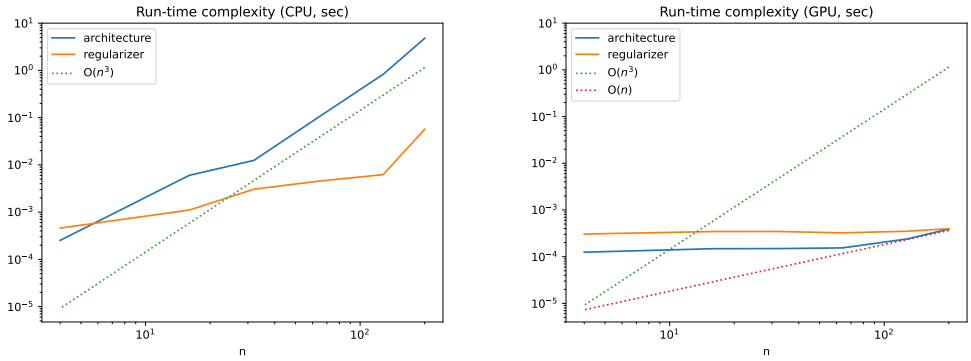

Figure 11: **Run-time complexity** for computing the HyperCube architecture (eq (4)) and regularizer (eq (6)) as functions of n. (Left) Run-time on CPU. (Right) Run-time on GPU (Tesla V100 16GB). Results are averaged over 100 runs.

F Alternative Tensor Factorizations

HyperCube distinguishes itself from conventional tensor factorization architectures, which typically employ lower-order, matrix factors for decomposition: *e.g.*, Tucker and CP decomposition. This difference is crucial for capturing the rich structure of binary operations.

Tucker Decomposition (Tucker, 1966) employs a core tensor M and three matrix factors:

$$T_{abc} = \frac{1}{n} \sum_{i,j,k} M_{ijk} A_{ai} B_{bj} C_{ck}, \tag{15}$$

While flexible, Tucker decomposition suffers from a critical limitation: In eq (15), the role of matrix factors is limited to simply mapping individual *external* indices to individual *internal* indices (e.g. A maps a to i). This presents a recursive challenge, since learning the algebraic relationships between (a, b, c) in T requires learning the relationships between (i, j, k) in M, which is not inherently simplifying the core learning problem. Consequently, Tucker decomposition severely overfits the training data and fails to generalize to unseen examples (Figure 12).

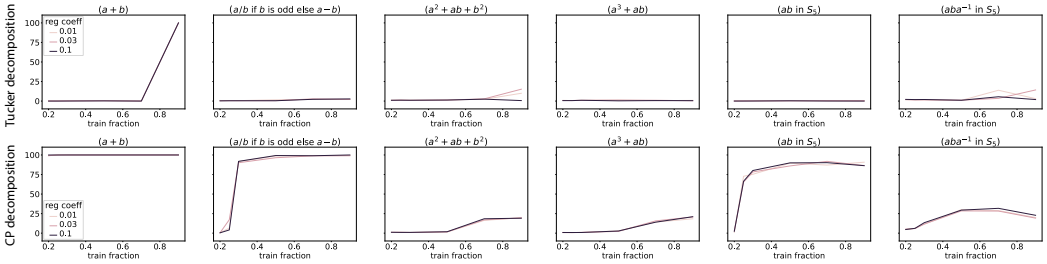

Figure 12: **Alternative Tensor Factorization Methods**: Test accuracy of (Top) Tucker and (Bottom) CP decomposition methods, trained across a range of L_2 regularization strengths.

CP Decomposition CP decomposition utilizes only matrix factors for decomposition:

$$T_{abc} = \frac{1}{n} \sum_k A_{ak} B_{bk} C_{ck}. \tag{16}$$

This is equivalent to[4] HyperCube with diagonal embeddings (*i.e.* $A_{aki} = A_{ak}\delta_{ki}$, $B_{bij} = B_{bi}\delta_{ij}$, $C_{cjk} = C_{cj}\delta_{jk}$), since

$$\sum_{ijk} A_{aki} B_{bij} C_{cjk} = \sum_{ijk} A_{ak} B_{bi} C_{cj} \delta_{ki} \delta_{ij} \delta_{jk} = \sum_k A_{ak} B_{bk} C_{ck}. \tag{17}$$

Therefore, while CP decomposition can fully capture commutative Abelian groups (e.g modular addition), which admit diagonal representations (*i.e.*, 1×1 irreps) in $K = \mathbb{C}$, it lacks the expressive power to capture more complex operations. In experiments (Figure 12), CP decomposition indeed shows reasonable performance only for the modular addition task, struggling to generalize to other structures in data.

G BAND-DIAGONAL HYPERCUBE

As mentioned above, HyperCube with diagonal embeddings lacks the capacity to effectively capture general group structures. However, the regular representation of a group generally decomposes into a direct sum of smaller irreducible representations, resulting in a sparse, block-diagonal matrix structure. Such block-diagonal structure can be effectively captured within the parameter space of *band-diagonal* matrices.

Therefore, to enhance the scalability of HyperCube, we explore the band-diagonal variant where the factor matrices are constrained to have a fixed bandwidth around the diagonal. This reduces the model's parameter count from $\mathcal{O}(n^3)$ to $\mathcal{O}(n^2)$, offering significant computational advantages.

Figure 13 compares the performance of the full HyperCube and the band-diagonal HyperCube with a bandwidth of 8 on a subset of tasks from Appendix B ($n = 97$ or 120). Remarkably, the band-diagonal version exhibits comparable performance to the full HyperCube model, demonstrating its effectiveness in capturing group structures even with a significantly reduced number of parameters. This result highlights the potential of band-diagonal HyperCube for scaling to larger problems.

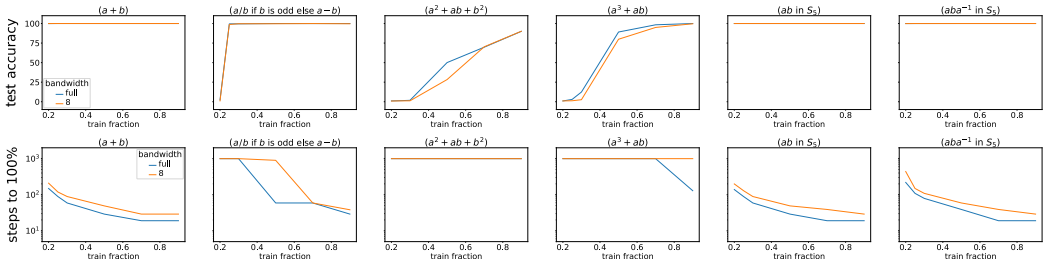

Figure 13: Full HyperCube vs Band-diagonal HyperCube model. (Top) final test accuracy, and (Bottom) steps to 100% test accuracy. lr $= 0.5$, reg coeff $\epsilon = 0.05$, init scale $= 1.0$.

[4]CP decomposition can also be viewed as a special case of Tucker decomposition with a fixed core tensor

$$M_{ijk} = 1 \quad \text{if } i = j = k, \quad 0 \quad \text{otherwise.}$$

H Deferred Proofs

H.1 Proof of Lemma 5.1 on Balanced Condition of HyperCube

Here, we derive the balanced condition eq (7). The gradient of the regularized loss $\mathcal{L} = \mathcal{L}_o(T; D) + \epsilon\mathcal{H}(A, B, C)$ is

$$\nabla_{A_a}\mathcal{L} = \frac{1}{n}((\nabla_{T_{abc}}\mathcal{L}_o)\, C_c^\dagger B_b^\dagger + 2\epsilon(A_a(B_bB_b^\dagger) + (C_c^\dagger C_c)A_a)), \tag{18}$$
$$\nabla_{B_b}\mathcal{L} = \frac{1}{n}((\nabla_{T_{abc}}\mathcal{L}_o)\, A_a^\dagger C_c^\dagger + 2\epsilon(B_b(C_cC_c^\dagger) + (A_a^\dagger A_a)B_b)),$$
$$\nabla_{C_c}\mathcal{L} = \frac{1}{n}((\nabla_{T_{abc}}\mathcal{L}_o)\, B_b^\dagger A_a^\dagger + 2\epsilon(C_c(A_aA_a^\dagger) + (B_b^\dagger B_b)C_c)),$$

where $\nabla_{A_a}\mathcal{L} \equiv \partial\mathcal{L}/\partial A_a$, $\nabla_{B_b}\mathcal{L} \equiv \partial\mathcal{L}/\partial B_b$, $\nabla_{C_c}\mathcal{L} \equiv \partial\mathcal{L}/\partial C_c$, and $\nabla_{T_{abc}}\mathcal{L}_o \equiv \partial\mathcal{L}_o/\partial T_{abc}$.

Define the *imbalances* as the differences of loss gradients:

$$\xi_I \equiv \frac{n}{2\epsilon}(A_a^\dagger(\nabla_{A_a}\mathcal{L}) - (\nabla_{B_b}\mathcal{L})B_b^\dagger) = A_a^\dagger(C_c^\dagger C_c)A_a - B_b(C_cC_c^\dagger)B_b^\dagger$$
$$\xi_J \equiv \frac{n}{2\epsilon}(B_b^\dagger(\nabla_{B_b}\mathcal{L}) - (\nabla_{C_c}\mathcal{L})C_c^\dagger) = B_b^\dagger(A_a^\dagger A_a)B_b - C_c(A_aA_a^\dagger)C_c^\dagger$$
$$\xi_K \equiv \frac{n}{2\epsilon}(C_c^\dagger(\nabla_{C_c}\mathcal{L}) - (\nabla_{A_a}\mathcal{L})A_a^\dagger) = C_c^\dagger(B_b^\dagger B_b)C_c - A_a(B_bB_b^\dagger)A_a^\dagger$$

Setting the gradient to zero yields the balanced condition at stationary points, $\xi_I = \xi_J = \xi_K = 0$, which proves Lemma 5.1. Note that imbalance terms are defined to cancel out the $\nabla_{T_{abc}}\mathcal{L}_o$ terms. Therefore, the balanced condition is independent of the loss function $\mathcal{L}_o$.

H.2 Proof of Lemma 5.4

Proof. The constraint on Frobenius norm can be integrated with the regularizer into an augmented loss via the Lagrange multiplier λ

$$\mathcal{H} + \lambda(\mathcal{F} - constant), \tag{19}$$

where $\mathcal{F} \equiv \frac{1}{n}\,\mathrm{Tr}\left[A_a^\dagger A_a + B_b^\dagger B_b + C_c^\dagger C_c\right]$ is the Frobenius norm .

The gradient of eq (19) with respect to A_a is proportional to

$$\nabla_{A_a}(\mathcal{H} + \lambda\mathcal{F}) \propto A_a(B_bB_b^\dagger) + (C_c^\dagger C_c)A_a + \lambda A_a. \tag{20}$$

In the case of C-unitary factors B and C, all terms in eq (20) become aligned to A_a, *i.e.*

$$\nabla_{A_a}(\mathcal{H} + \lambda\mathcal{F}) \propto (\alpha_B^2 + \alpha_C^2 + \lambda)A_a. \tag{21}$$

and thus an appropriate value for the Lagrange multiplier λ can be found to vanish the gradient, which confirms stationarity. This result also applies to gradient with respect to B_b and C_c by the symmetry of parameterization. □

H.3 Persistence of Group Representation

The following lemma demonstrates a key property of our model's convergence behavior: once a group representation is learned, the solution remains within this representational form throughout optimization.

Lemma H.1. *Let D represent a group operation table. Once gradient descent of the regularized loss eq* (5) *converges to a group representation (including scalar multiples), i.e.*

$$A_a = \alpha_{A_a}\varrho(a),\ B_b = \alpha_{B_b}\varrho(b),\ C_c = \alpha_{C_c}\varrho(c)^\dagger, \tag{22}$$

the solution remains within this representation form.

Proof. For the squared loss

$$\mathcal{L}_o(T; D) = \sum_{(a,b,c)\in\Omega_{\text{train}}} (T_{abc} - D_{abc})^2, \tag{23}$$

the gradient with respect to A_a eq (18) becomes

$$\nabla_{A_a}\mathcal{L} = \frac{1}{n}(\Delta_{abc}M_{abc}C_c^\dagger B_b^\dagger + \epsilon(A_a(B_bB_b^\dagger) + (C_c^\dagger C_c)A_a)) \tag{24}$$

where $\Delta \equiv T - D$ is the constraint error, and M is the mask indicating observed entries in the train set.

Substituting the group representation form eq (22) into eq (24), we get:

$$\frac{1}{n}\epsilon(A_a(B_bB_b^\dagger) + (C_c^\dagger C_c)A_a) = 2\epsilon\alpha_{A_a}\alpha^2\varrho(a), \tag{25}$$

for the last two terms, where $\alpha^2 = \sum_b \alpha_{B_b}^2/n = \sum_c \alpha_{C_c}^2/n$.

Since the product tensor is

$$T_{abc} = \frac{1}{n}\operatorname{Tr}[A_aB_bC_c] = \frac{1}{n}\alpha_{A_a}\alpha_{B_b}\alpha_{C_c}\operatorname{Tr}[\varrho(a)\varrho(b)\varrho(c)^\dagger] = \alpha_{A_a}\alpha_{B_b}\alpha_{C_c}D_{abc},$$

and $D_{abc} = \delta_{a\circ b,c} = \delta_{a,c\circ b^{-1}}$ (δ is the Kronecker delta function), the first term in eq (24) becomes

$$\begin{aligned}\frac{1}{n}\sum_{b,c}\Delta_{abc}M_{abc}C_c^\dagger B_b^\dagger &= \frac{1}{n}\sum_{b,c}\delta_{a\circ b,c}M_{abc}(\alpha_{A_a}\alpha_{B_b}\alpha_{C_c} - 1)\alpha_{B_b}\alpha_{C_c}\varrho(c\circ b^{-1}) \\ &= \frac{1}{n}\sum_{b} M_{ab(a\circ b)}(\alpha_{A_a}\alpha_{B_b}\alpha_{C_{a\circ b}} - 1)\alpha_{B_b}\alpha_{C_{a\circ b}}\varrho(a).\end{aligned} \tag{26}$$

Note that both eq (26) and eq (25) are proportional to $\varrho(a)$. Consequently, we have $\nabla_{A_a}\mathcal{L} \propto \varrho(a)$. Similar results for other factors can also be derived: $\nabla_{B_b}\mathcal{L} \propto \varrho(b)$, and $\nabla_{C_c}\mathcal{L} \propto \varrho(c)^\dagger$. This implies that gradient descent preserves the form of the group representation (eq (22)), only updating the coefficients $\alpha_{A_a}, \alpha_{B_b}, \alpha_{C_c}$. □

Effect of ϵ-Scheduler Lemma H.1 holds true even when ϵ gets modified by ϵ-scheduler, which reduces ϵ to 0. In this case, the coefficients converge to $\alpha_{A_a} = \alpha_{B_b} = \alpha_{C_c} = 1$, resulting in the exact group representation form eq (9).

I GROUP CONVOLUTION AND FOURIER TRANSFORM

I.1 FOURIER TRANSFORM ON GROUPS

The Fourier transform of a function $f : G \to \mathbb{R}$ at a representation $\varrho : G \to \mathrm{GL}(d_\varrho, \mathbb{R})$ of G is

$$\hat{f}(\varrho) = \sum_{g \in G} f(g)\varrho(g). \tag{27}$$

For each representation ϱ of G, $\hat{f}(\varrho)$ is a $d_\varrho \times d_\varrho$ matrix, where d_ϱ is the degree of ϱ.

I.2 DUAL GROUP

Let $\hat{G}$ be a complete set indexing the irreducible representations of G up to isomorphism, called the *dual group*, thus for each ξ we have an irreducible representation $\varrho_\xi : G \to U(V_\xi)$, and every irreducible representation is isomorphic to exactly one ϱ_ξ.

I.3 INVERSE FOURIER TRANSFORM

The inverse Fourier transform at an element g of G is given by

$$f(g) = \frac{1}{|G|} \sum_{\xi \in \hat{G}} d_{\varrho_\xi} \operatorname{Tr}\left[\varrho_\xi(g^{-1})\hat{f}(\varrho_\xi)\right]. \tag{28}$$

where the summation goes over the complete set of irreps in $\hat{G}$.

I.4 GROUP CONVOLUTION

The convolution of two functions over a finite group $f, g : G \to \mathbb{R}$ is defined as

$$(f * h)(c) \equiv \sum_{b \in G} f\left(c \circ b^{-1}\right) h(b) \tag{29}$$

I.5 FOURIER TRANSFORM OF GROUP CONVOLUTION

Fourier transform of a convolution at any representation ϱ of G is given by the matrix multiplication

$$\widehat{f * h}(\varrho) = \hat{f}(\varrho)\hat{h}(\varrho). \tag{30}$$

In other words, in Fourier representation, the group convolution is simply implemented by the matrix multiplication.

Proof.

$$\widehat{f * h}(\varrho) \equiv \sum_c \varrho(c) \sum_b f(c \circ b^{-1})h(b) \tag{31}$$

$$= \sum_c \varrho(c) \sum_{a,b} f(a)h(b)\delta_{(a, c \circ b^{-1})} \tag{32}$$

$$= \sum_{a,b} f(a)h(b) \sum_c \varrho(c)\delta_{(a \circ b, c)} \tag{33}$$

$$= \sum_{a,b} f(a)h(b)\varrho(a \circ b) \tag{34}$$

$$= \sum_a f(a)\varrho(a) \sum_b h(b)\varrho(b) \tag{35}$$

$$= \hat{f}(\varrho)\hat{h}(\varrho). \tag{36}$$

where δ is the Kronecker delta function, and the equivalence between $a = c \circ b^{-1}$ and $a \circ b = c$ is used between the second and the third equality. □

J GROUP CONVOLUTION AND FOURIER TRANSFORM IN HYPERCUBE

HyperCube shares a close connection with group convolution and Fourier transform. On finite groups, the Fourier transform generalizes classical Fourier analysis to functions defined on the group: $f : G \to \mathbb{R}$. Instead of decomposing by frequency, it uses the group's irreducible representations $\{\varrho_\xi\}$, where ξ indexes the irreps (See Appendix I.2). A function's Fourier component at ξ is defined as:

$$\hat{f}_\xi \equiv \sum_{g \in G} f(g)\varrho_\xi(g). \tag{37}$$

Fourier Transform in HyperCube The Fourier transform perspective offers a new way to understand how HyperCube with a group representation eq (9) processes general input vectors. Consider a vector f representing a function, *i.e.*, $f_g = f(g)$. Contracting f with a model factor A (or B) yields:

$$\hat{f} \equiv f_g A_g = \sum_{g \in G} f(g)\varrho(g), \tag{38}$$

which calculates the Fourier transform of f using the regular representation ϱ. As ϱ contains all irreps of the group, $\hat{f}$ holds the complete set of Fourier components. Conversely, contracting $\hat{f}$ with $\varrho^\dagger$ (*i.e.* factor C) performs the *inverse Fourier transform*:

$$\frac{1}{n}\operatorname{Tr}[\hat{f}C_g] = \frac{1}{n}\sum_{g' \in G} f_{g'} \operatorname{Tr}[\varrho(g')\varrho(g)^\dagger] = f_g, \tag{39}$$

where eq (2) is used. This reveals that the factor tensors generalize the discrete Fourier transform (DFT) matrix, allowing the model to map signals between the group space and its Fourier (frequency) space representations.

Through the lens of Fourier transform, we can understand how the model eq (10) processes general input vectors (f and h): it calculates their Fourier transforms ($\hat{f}, \hat{h}$), multiplies them in the Fourier domain ($\hat{f}\hat{h}$), and applies the inverse Fourier transform. Remarkably, this process is equivalent to performing group convolution ($f * h$). This is because the linearized group operation (Section 4.1) naturally entails group convolution (see Appendix J.1,J.2).

This connection reveals a profound discovery: HyperCube's ability to learn symbolic operations is fundamentally the same as learning the core structure of group convolutions. This means HyperCube can automatically discover the essential architecture needed for equivariant networks, without the need to hand-design them. This finding highlights the broad potential of HyperCube's inductive bias, extending its applicability beyond the realm of symbolic operations.

J.1 REINTERPRETING HYPERCUBE'S COMPUTATION

HyperCube equipped with group representation eq (10) processes general input vectors f and h as

$$\begin{aligned} f_a h_b T_{abc} &= \frac{1}{n}\sum_a \sum_b f(a)h(b)\operatorname{Tr}\left[\varrho(a)\varrho(b)\varrho(c)^\dagger\right] \\ &= \frac{1}{n}\operatorname{Tr}\left[\left(\sum_a \varrho(a)f(a)\right)\left(\sum_b \varrho(b)h(b)\right)\varrho(c)^\dagger\right] \\ &= \frac{1}{n}\operatorname{Tr}[(\hat{f}\hat{h})\varrho(c)^\dagger] = \frac{1}{n}\operatorname{Tr}[\widehat{f * h}\,\varrho(c)^\dagger] \\ &= (f * h)_c. \end{aligned} \tag{40}$$

Therefore, the model calculates the Fourier transform of the inputs ($\hat{f}$ and $\hat{h}$), multiplies them in the Fourier domain ($\hat{f}\hat{h}$), and applies the inverse Fourier transform, which is equivalent to the group convolution, as shown in Appendix I.5.

J.2 GROUP CONVOLUTION BY D

Here we show that the linearized group operation D in Section 4.1 is equivalent to the group convolution in Appendix I.5.

Consider contracting the data tensor D with two functions $f, h \in G$, as

$$f_a h_b D_{abc} = \sum_{ab} f(a)h(b)\delta_{(a,c\circ b^{-1})} = \sum_{b} f(c \circ b^{-1})h(b) \equiv (f * h)(c), \tag{41}$$

which computes the group convolution between f and h, similar to eq (40). Here, we used $D_{abc} = \delta_{(a\circ b,c)} = \delta_{(a,c\circ b^{-1})}$.

K SUPPLEMENTARY FIGURES FOR SECTION 6

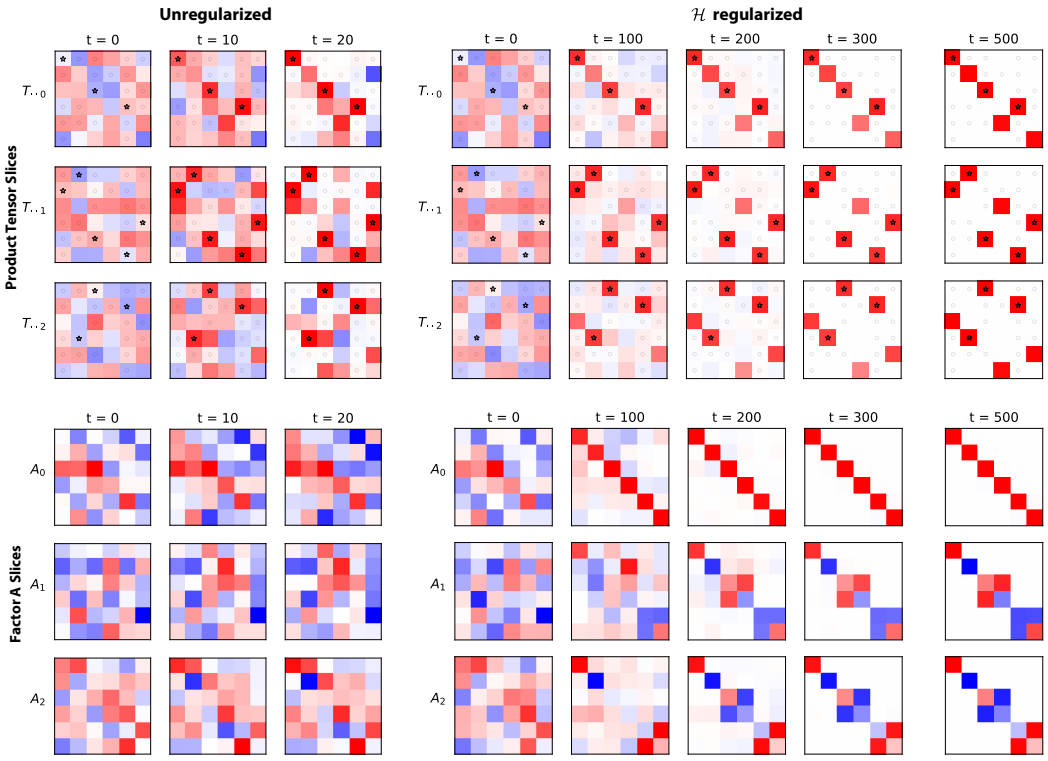

Figure 14: Visualization of the end-to-end model tensor T and the factor A over the training iteration steps on the symmetric group S_3 task in Sec 6. Only the first three slices of the tensors are shown. (Top) End-to-end model tensor T: In the un-regularized case, the model tensor quickly converges to fit the observed data tensor entries in the training dataset (marked by stars and circles), but not in the test dataset. The $\mathcal{H}$-regularized model converges to a generalizing solution around $t = 200$. It accurately recovers D when the regularization diminishes around $t = 400$ ($\epsilon \to 0$). (Bottom) Factor tensor A. The unregularized model shows minimal changes from random initial values, while $\mathcal{H}$-regularized model shows significant internal restructuring. Shown in the block-diagonalizing coordinate. See Fig 15 (Bottom). (color scheme: red=1, white=0, blue=-1.)

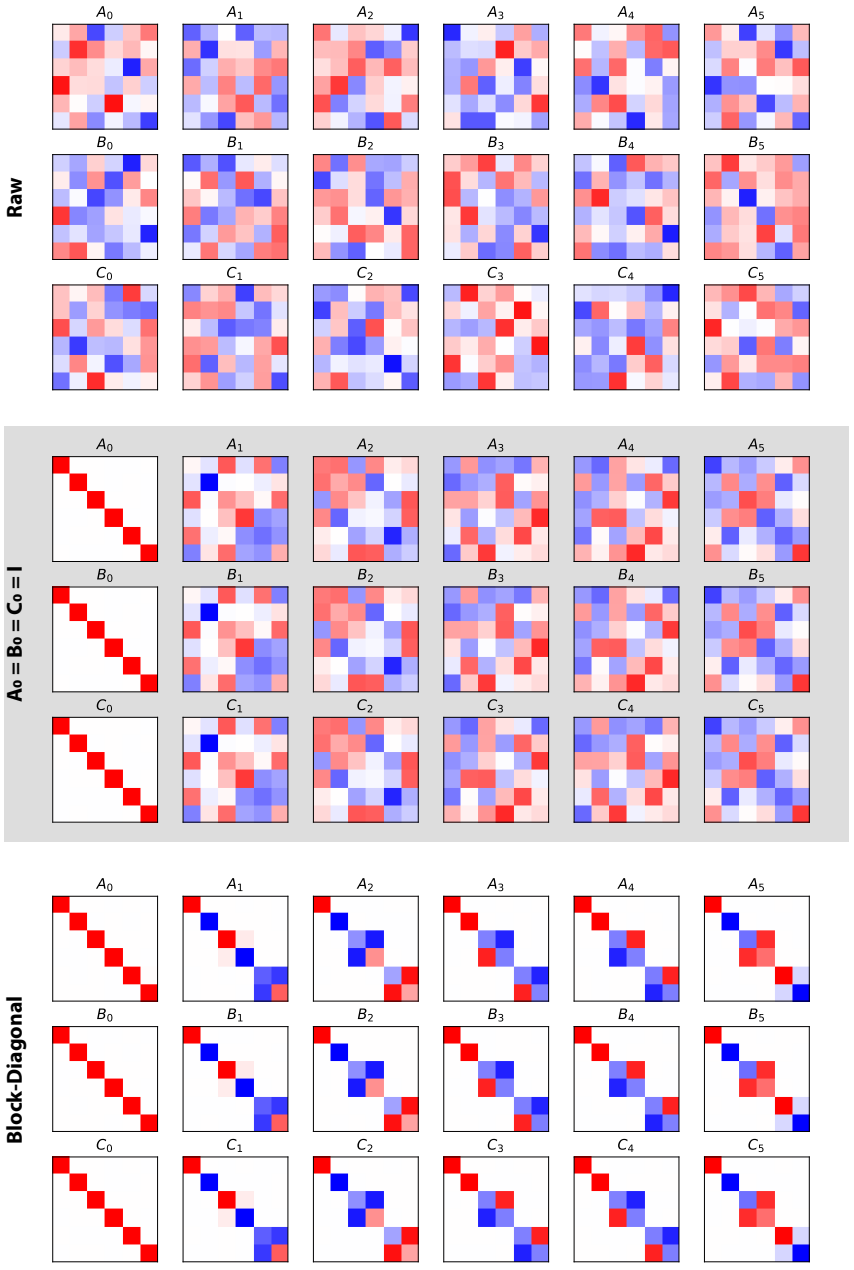

Figure 15: Learned factors of the $\mathcal{H}$ regularized model trained on the S_3 group. (Top) Raw factor weights shown in their native coordinate representation. (Middle) Unitary basis change as described in Sec 4.4 with $M_I = I$, $M_K = A_0$, $M_J = B_0^\dagger$, such that $\tilde{A}_0 = \tilde{B}_0 = \tilde{C}_0 = I$. Note that the factors share same weights (up to transpose in factor $\tilde{C}$). (Bottom) Factors represented in a block-diagonalizing basis coordinate, revealing the decomposition into direct sum of irreducible representations (irreps). (color scheme: red=1, white=0, blue=-1.)

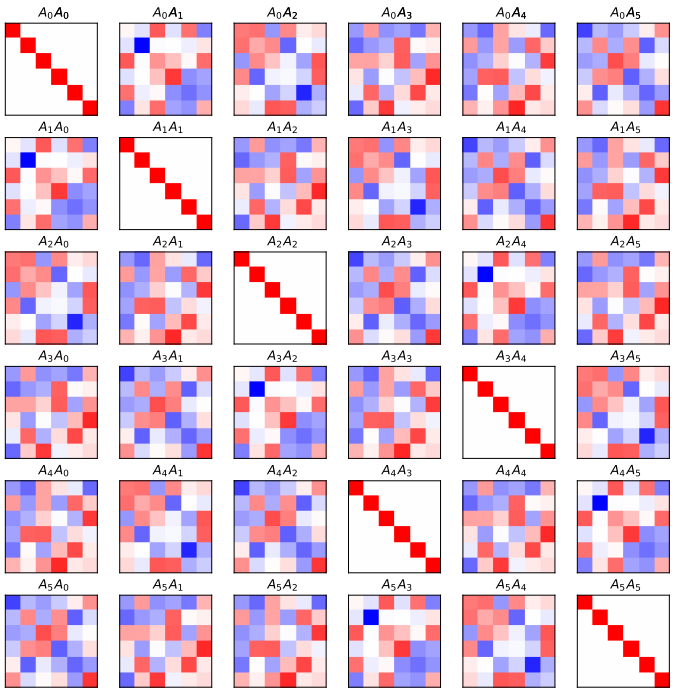

Figure 16: Multiplication table of matrix slices of factor A from the mid panel of Fig 15. Note that this table share the same structure as the Cayley table of the symmetric group S_3 in Fig 2A. (color scheme: red=1, white=0, blue=-1.)

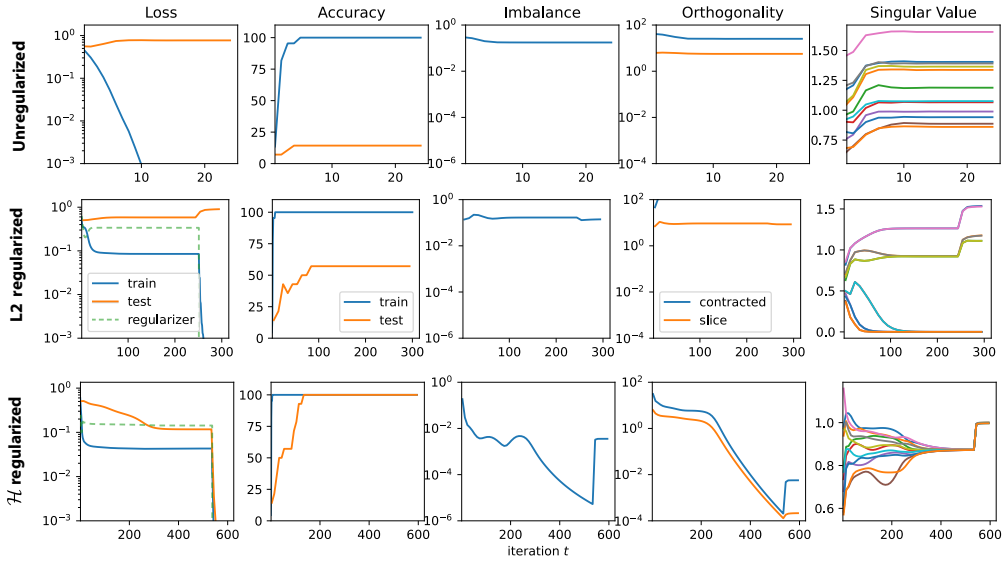

Figure 17: Optimization trajectories on the modular addition (cyclic group C_6) dataset, with 60% of the Cayley table used as train dataset (see Fig 18). (Top) Unregularized, (Middle) L_2-regularized, and (Bottom) $\mathcal{H}$-regularized training. The L_2-regularized model only achieves $\sim$60% test accuracy.

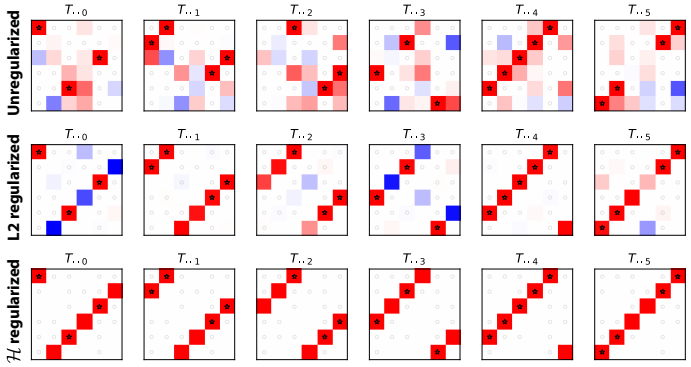

Figure 18: Visualization of end-to-end model tensor T trained on the modular addition (cyclic group C_6) under different regularization strategies (see Fig 17). The observed training data are marked by asterisks (1s) and circles (0s). Only the $\mathcal{H}$-regularized model perfectly recovers the data tensor D. (color scheme: red=1, white=0, blue=-1.)

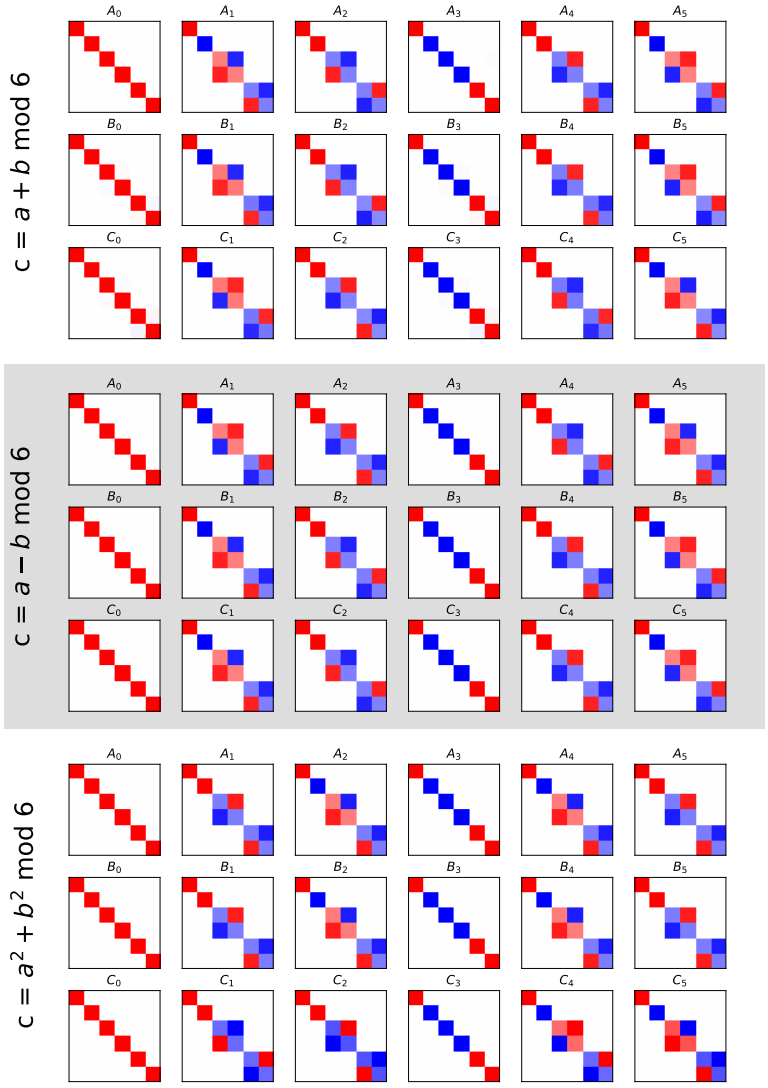

Figure 19: Visualization of factors trained on small Cayley tables from Figure 2. (Top) $c = a + b$ mod 6, satisfying $A_g = B_g = C_g^\dagger = \varrho(g)$. (Middle) $c = a - b$ mod 6, satisfying $A_g^\dagger = B_g = C_g = \varrho(g)$. (Bottom) $c = a^2 + b^2$ mod 6, which exhibits the same representation as modular addition for elements with unique inverses (e.g., $g = 0, 3$). For others, it learns *duplicate* representations reflecting the periodicity of squaring modulo 6: *e.g.*, $A_2 = A_4$ and $A_1 = A_5$, since $2^2 = 4^2$ and $1^2 = 5^2$. (color scheme: red=1, white=0, blue=-1.)